

Detection and characterization of extrasolar planets: the transit method

Claire Moutou¹ and Frédéric Pont²

¹ *Laboratoire d'Astrophysique de Marseille, Marseille, France, Claire.Moutou@oamp.fr,*

² *Observatoire de Genève, Versoix, Switzerland, Frederic.Pont@obs.unige.ch*

Abstract. Exoplanets can be detected by the *transit method* when the star, planet and observer are aligned. The transits translate into a shallow dip in the stellar light curve. When combined with radial velocity measurements, the transit method permits the determination of a planet's mass, radius and density. In this chapter we describe the main features of transit light curves, some issues about the method and we compare its capabilities and observables to other methods for the detection and characterisation of extrasolar planets.

Contents

1. Introduction	57
2. The transit method	58
2.1 Principles	58
2.2 Measured parameters	58
Transit depth.	59
Transit duration.	59
Ingress duration.	60
2.3 Elliptical orbits	60
3. Transit detection	61
3.1 Survey type and targets	62
3.2 Temporal sampling and length of the survey	63
3.3 Photometric accuracy	63
3.4 Detection algorithms	64
3.5 Two examples: OGLE and COROT	65

3.6	Biases of the method	66
3.7	Eclipsing binaries and false positives	66
	Grazing binaries	67
	Small-radius stellar companion	67
	Eclipsing binaries which light is diluted by a third star	69
	False positives	69
3.8	Detection threshold	69
4.	Planet characterisation	70
4.1	Planet confirmation	70
4.2	Light curves of RV planets	71
4.3	The mass-radius diagram	73
4.4	Further analysis of transiting planets	73
	Thermal emission of the transiting planet.	73
	Reflected light/Albedo.	74
	Satellites and rings.	75
	The Rossiter-Mc Laughlin effect.	75
	Detection of the extended planetary atmosphere.	75
5.	Conclusion	76

1. Introduction

Indirect methods are so far the most efficient ways to detect and characterise extrasolar planets. The radial velocity (RV) method (see Bouchy, this volume) provided most of the known planets (about 160 in October 2005), while the transit method, presented here, allowed the discovery of six planets and the confirmation/characterisation of three RV planets.

The transit method met its first success in 1999 with the transit observation of the RV planet HD 209458b (ref. 17, 30 and Fig. 1, left). It then became popular for two reasons: 1) the detection of a planetary transit around a bright star requires a telescope as small as 20-cm in diameter, and many transit surveys were initiated after this first success; 2) studies of a planetary system seen edge-on is much richer than for systems at any inclination, because the radius and the mass are directly measured.

After the current success of ground-based transit searches like OGLE, major transit discoveries are expected from space, or already obtained (Fig. 1, right). The future space-borne projects CoRoT and *Kepler* are the next milestones to be considered, since they could discover the first Earth-sized planets, using the transit method.

This paper presents the transit method and its measured parameters (Sec. 1), the principle of transit detection surveys (Sec. 2) and the characterisation of transiting planets (Sec. 3).

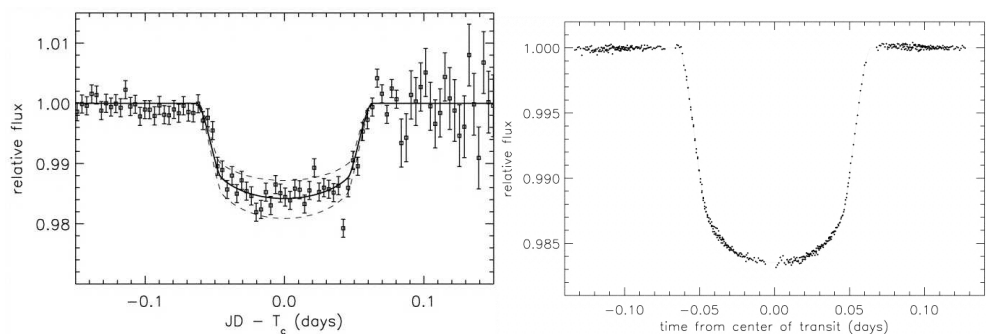


Figure 1.: *Left: the light curve of HD 209458, showing the first observed planetary transit (17). Right: the same system observed by HST/STIS, the highest signal-to-noise ratio transit light curve observed so far (15).*

2. The transit method

2.1 Principles

The transit method consists in detecting the shallow dip in a stellar light curve when a planet crosses the line of sight towards its host star during its revolution. It thus requires an almost perfect alignment between the observer, the planet, and the star. The transit appears periodically, with a period equal to the revolution period of the planet. The probability \mathcal{P}_{tr} for a planetary system to show a transit is a direct relation to the star radius R and the semi-major axis a : $\mathcal{P}_{tr} = R/a$.

Applying this equation to the solar system, it follows that the Earth in front of the Sun has a 1/214 probability to produce a transit for a distant observer; for Jupiter the value is 1/1100. It implies that, assuming 1% of stars have a Jupiter, one transit may occur, every 12 years (the orbital period of Jupiter) if 100,000 stars are monitored! Such events are too rare to be observed, even if a Jupiter transit with a 1% depth and 30 hour duration would in principle be detectable from the ground. With the discovery of the “hot Jupiter” class of planets in 1995, the prospects of detecting exoplanets by looking for transits improved dramatically. For 51 Peg b, the transit probability is about 10% and transit events recur every $\simeq 4$ days. The order of magnitude of the number of stars to be monitored for detecting a hot Jupiter by the transit method is 1,000, within easy reach of any wide-field CCD imaging.

A planetary system observed edge-on, as in the case of transiting systems, also offers the geometry for the strongest radial velocity (RV) signal to be observed; moreover, the “ $\sin i$ ” indetermination related to the velocimetric method disappears because the orbital angle is known and the measured RV amplitude is directly related to the true planet mass. The synergy of both transit and RV methods will be further discussed in Section 4.

2.2 Measured parameters

The planetary transit measured in the stellar light curve is mainly described by three parameters: its depth, its duration, and its shape. Depending on the latitude of the transit on the stellar disk, the transit light curve will be U-shaped (central occultation) or V-shaped (grazing occultation). Quantitatively, the related parameter is the duration of the ingress and egress (alternatively, the duration of the flat bottom of the transit).

Let us calculate these parameters in the simplified case of a circular orbit and a stellar disc of uniform brightness. The sketch of a planetary transit is given in Figure 2. Ingress (resp. egress) is defined as the phase

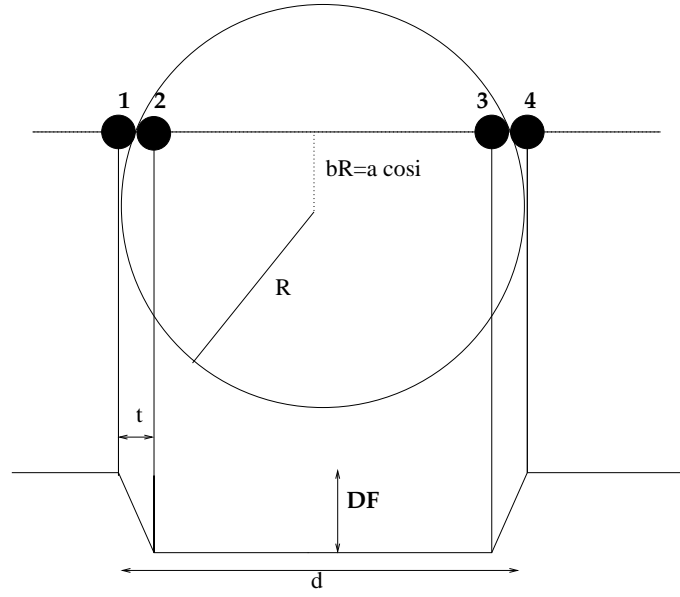


Figure 2.: Sketch of a planetary transit.

from contact 1 (resp. 3) to contact 2 (resp. 4). The "flat bottom" corresponds to phases 2 to 3.

Transit depth. The depth of the transit is related to the star and planet radii (R and r respectively):

$$\Delta F = \frac{F_{off} - F_{on}}{F_{off}} = (r/R)^2 \quad (1)$$

F_{off} is the observed stellar flux out of transit, and F_{on} is the observed flux during transit. This formula neglects the phenomenon known as *limb darkening*, i.e. the fact that stars appear slightly brighter in their center than near the edge. Taking limb darkening into account makes the transits slightly deeper than $(r/R)^2$, and gives the lightcurve a more rounded shape (see Figure 3).

Transit duration. The total duration of the transit, for a circular orbit, is related to the orbital parameters and to the star radius:

$$d \simeq \frac{PR}{\pi a} \sqrt{\left(1 + \frac{r}{R}\right)^2 - \left(\frac{a}{R} \cos i\right)^2} \quad (2)$$

Parameter P is the orbital period, in the same unit as d , and a is the orbital radius in the same unit as R and r ; i is the inclination of the orbit.

The expression $\frac{a}{R} \cos i$ is the impact parameter, b , the projected distance of the planet's center to the star's equator in units of star's radius. The exact formalism for the transit duration is given in ref. 54, while more user-friendly equations are (as expressed against period or semi-major axis):

$$d \simeq 13.0 \sqrt{(1 - b^2)} \frac{R}{M^{1/2}} a^{1/2} \simeq 1.8 \sqrt{(1 - b^2)} \frac{R}{M^{1/3}} P^{1/3} \quad (3)$$

where M is the star's mass, the mass of the planet being negligible. Contrarily to Eq. 2, d is here in hours, P in days, a in astronomical unit, and R and M are both in solar units.

Ingress duration. Another temporal parameter of the transit is the duration of the ingress or egress:

$$t \simeq d \frac{r}{R} \sqrt{1 - b^2} \quad (4)$$

One may also consider the transit shape by deriving the ratio of the durations of the flat bottom (t_F) over the total transit (d):

$$\left(\frac{t_F}{d}\right)^2 = \frac{(1 - \frac{r}{R})^2 - (\frac{a}{R} \cos i)^2}{(1 + \frac{r}{R})^2 - (\frac{a}{R} \cos i)^2} \quad (5)$$

The three equations describing a planetary transit (depth, total duration and ingress duration), can be used to constrain four unknown parameters of the system: r , R , M , b . The star's mass and radius may be independently constrained by other observations, specifically high-resolution spectroscopy, as well as with stellar evolution models. For instance, for low-mass stars, $M \propto R$ is a fairly good approximation.

2.3 Elliptical orbits

Due to the higher probability of detecting transits of short-period planets, which orbits are rapidly circularised by tidal effects, it is usually sufficient to consider the transit formalism for circular orbits, as given above. However, the eccentricity of even close-in planets is sometimes above 0.1. Also, future space missions will be able to observe the same stars for years (e.g. *Kepler*, 9), and thus to search for planets with longer periods (and thus larger eccentricities). It will then be important to handle the case of elliptical orbits. In that case, the transit duration (and shape) depends on the planet position on its orbits (hereafter, the phase angle ϕ , with respect to the periastron of the ellipse). Figure 4 shows how the transit duration evolves with orbital eccentricity and

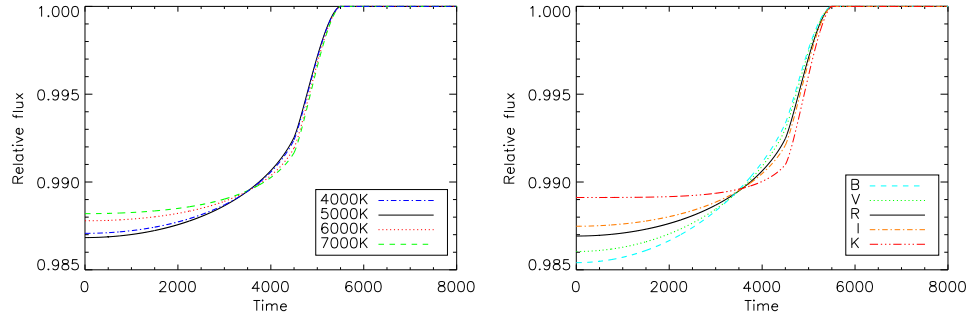


Figure 3.: *Left: Modelisation of a planetary transit (in this example, Saturn passing the Solar disc at 88° inclination) with various limb-darkening coefficients, corresponding to dwarf stars of effective temperatures 4000 to 7000K. Right: the same, in various photometric bands. The transit light curves have been calculated using the routine of Mandel and Agol (36).*

phase angle. The transit duration in an elliptical orbit with eccentricity e is (58):

$$d = 2 \sqrt{\frac{1 - (\rho \cos i)^2}{(R + r)^2}} (R + r) \frac{\sqrt{1 - e^2}}{1 + e \cos \phi} \left(\frac{P}{2\pi GM} \right)^{1/3} \quad (6)$$

where G is the gravitational constant, and ρ is the star-planet distance at the time of the transit, corresponding to a phase angle ϕ .

Another effect of an eccentricity greater than zero is to change the timing of the secondary eclipse. If $t_1 - t_2$ is the time interval between the primary and secondary eclipses, then we get (19):

$$\frac{\pi}{2P} (t_1 - t_2 - P/2) \simeq e \cos \omega \quad (7)$$

The exact timing of a secondary eclipse may thus be derived if the orbit is precisely known, or alternatively, the observation of the secondary eclipse may provide an accurate estimate of the orbital eccentricity (as in ref. 19).

3. Transit detection

The success expected in detecting planetary transits is based on several parameters, among which: the number of monitored stars and their type; the temporal sampling and total duration of the observations; the

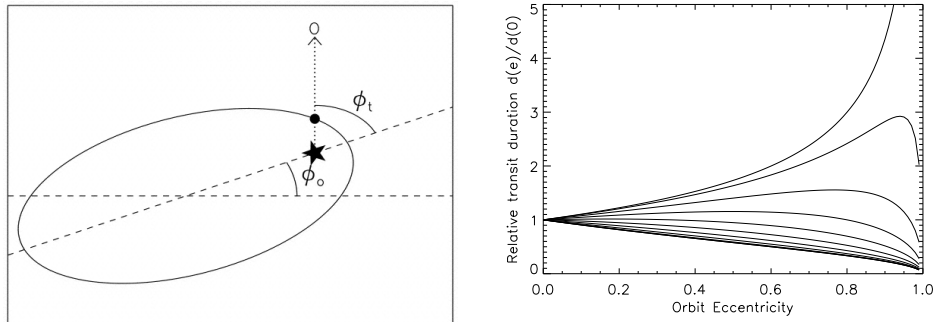


Figure 4.: *Left: orbital geometry showing the phase angle (from 58). Right: the range of transit durations is shown as a function of the orbital eccentricity, for a Jupiter-sized planet crossing the Solar disc ($b = 0$, $P = 10$ days). The thick lines show the largest (resp. shortest) durations corresponding to a transit occurring at apastron (resp. periastron). Several intermediate geometrical positions are also plotted.*

photometric accuracy and sensitivity; the algorithms used for detrending¹ the light curves and for detecting shallow and periodic box-shaped events.

3.1 Survey type and targets

The discovery in 1999 of the first transiting exoplanet HD 209458b triggered a large number of transit detection surveys. Schematically, there are four types of surveys: shallow, wide-angle surveys; intermediate surveys in the Galactic plane; deep and narrow-angle surveys; and surveys in clusters. They all include a large number of target stars due to the low probability of catching a transit (about 0.1% for short period planets).

Among the shallow, wide-angle surveys, only the TrES collaboration announced a confirmed planet detection so far (4), despite the larger expectations of such programs (review by Horne, 31). Deep surveys (37), as performed with HST or on 8m-class telescopes, and surveys towards clusters (14, 39, 55, 13, 29) have not announced yet the discovery of any planet. This lack of detections probably results from the inadequate accounting for stellar populations, contamination sources, and real in-

¹detrending: removing medium-term variations in the light curve (due for instance to systematic trends in the photometric errors and intrinsic variability of the target stars).

strumental capabilities, including systematic residuals in the photometry (see Section 3.8) as well as the practical difficulties of accumulating a sufficient number of nights of observation. The search for planets in the globular cluster 47 Tuc with the Hubble Space Telescope, leading to no detection, comforted the observation that planets are more frequent in metallicity-enriched stellar environments (27) and therefore very rare in the metal-deficient globular clusters. Transit searches in metal-rich open clusters were also negative (e.g. 13).

An optimal magnitude range for transit surveys seems to be $\simeq 10$ –16. It allows to get many thousands of stars in a typical wide field of 1 square degree. It also permits spectroscopic follow-up and then confirmation of the transit candidates. Galactic fields with the largest proportion of main-sequence stars are optimal, since giant stars are too large for planetary transits to be detectable.

3.2 Temporal sampling and length of the survey

The typical duration of planetary transits is 1 to 6 hours (Section 2.1) for periods less than 25 days, or transit probability more than 1% for the smallest stars. Detectivity simulations have shown that observation time series of more than about 5 times the orbital period are necessary to have a good probability of detection of transits, in good weather conditions (43). Thus, the detection of hot planets (P up to 10 days) from the ground requires a minimum of 50 nights of observation.

A correct determination of the transit shape requires a time sampling of about 1 min, in order to get about 10–20 data points during the critical ingress and egress periods.

3.3 Photometric accuracy

The final accuracy obtained on a photometric light curve results from contributions of the photon noise, the background or stellar vicinity, and the systematics such as airmass, seeing, twilight and extinction effects. The photon noise is often not the limiting source of noise in the search for transit-like signals. The presence of a faint neighbour star combined with seeing variations may induce photometric fluctuations at time scales of few hours. Airmass and twilight have impacts on the light curve with a ~ 8 -hour time-scale but seeing variation may be rapid and wrongly identified as an ingress/egress. Colour terms may be corrected by cross-referencing light curves from stars of similar colours. A tool was recently designed to correct all such effects by grouping stars with similar patterns and subtracting systematics in light curves (56).

In wide transit-search surveys, photometric accuracies of better than 10 mmag are commonly achieved (61). For photometric follow-up obser-

vations of detected transits, an even higher accuracy can be obtained with good spatial resolution, using image subtraction (2, 3) and/or careful calibration with reference stars: typical values of 1 mmag can then be obtained from ground-based observatories (e.g. 40) and 0.1 mmag from space (15).

3.4 Detection algorithms

The transit detection algorithms may use the two main characteristics of transits: their box shape, encircled by "flat" areas of longer duration, and their repeatability. They should be sensitive enough to retrieve the shallow transits, while not producing too many false alarms. Hereafter we quickly review the different methods that have been adapted from classical mathematical tools in view of detecting planetary transits.

Using Fourier analysis of the light curve does not suit the transit detection problem, because of the extreme concentration in time of the transit event (the ratio of the transit duration over period is typically a few percents), and the presence of gaps in the light curve, especially for ground-based transit observations (32, 7). In the frequency domain, the transit energy is not highly concentrated and is masked by observational noise. The detection of transits is thus easier in the time domain, or in a specific wavelet domain that includes the time confinement of the transit events.

Bayesian methods have been applied to the transit search: 1) in the Fourier space, maximizing the likelihood function with a parameter corresponding to the frequency of the signal period (22), 2) or in the time domain, assuming square-shaped transits (1).

The best performances are achieved with the following methods: matched filtering and box-fitting algorithms. The matched filter is a powerful tool which is optimal in case of white gaussian noise. The stellar light curve is correlated with a simulated transit template curve, the parameters of which (epoch, period and duration of transits) are optimized by maximizing the correlation function. A statistical analysis of the correlation products is necessary to estimate the false alarm rate and assess the confidence level of the obtained maximum (32). The box-fitting algorithm or BLS (Box Least Square, 35) utilises the anticipated squared shape of the transit signal. It performs direct least-square fits of step functions to the signal, after folding at several trial periods. The transit shape is approximated by a two-level signal, i.e. the gradual light dip during ingress/egress is ignored, but such an approximation is valid for a detection tool. It performs well on long time series, including many transits of a given planet, and in presence of strong observational noise. A comparison of different transit detection algorithms was recently done (57) and showed that the matched filter, the BLS and slight variations of

them are the best tools; several types of algorithms should be applied to a given time series, as their relative performance depends on the actual transit signal and noise sources present.

Finally, one should consider the very significant step of detrending the light curves before applying detection tools. This is required to remove systematics or variability at a level several times the transit signal. The blind test performed on simulated light curves in the context of CoRoT has shown the importance of the denoising step, and has illustrated the highest performance of a harmonics-fitting detrending coupled with the BLS detection (41).

3.5 Two examples: OGLE and COROT

Let us focus now on two programs which are intermediate in terms of field of view and magnitude depth, the OGLE experiment and the future CoRoT satellite.

The OGLE experiment is based on observations performed in Las Campanas in Chile, on a 1.3m telescope which dedicates ~ 60 nights per year to the photometric monitoring of crowded stellar fields in the Galactic disc. The field of view is 25×25 arcmin and more than 100,000 stars are observed. 137 transit candidates with a depth 0.6-8% were announced in 2002 and 2003 (60, 61, 62). The spectroscopic follow-up of the 60 most promising candidates showed that only five were planetary transits (see Table 1). Despite the large number of polluting binaries among the transit candidates, the OGLE experiment is the most successful survey of planetary transits conducted so far. It has put emphasis on the necessity of a thorough RV follow-up of transiting candidates for confirmation. It also revealed a new class of exoplanets with periods less than 2 days, the “very hot jupiters” that were not detected yet by the RV method (33, 10). The transit method is even more biased towards the very short periods than the velocimetric method (transit probability and detection rate are higher). The success of the OGLE transit search and its RV follow-up throws some doubt on the usefulness of deep transit searches, as their targets will be too faint for any spectroscopic observations: no possible accurate determination of the stellar parameters (which often limits the accuracy in deriving planetary parameters), no confirmation of the planetary nature of the transit (as opposed to eclipsing binary stars), and no measurement of the planet mass.

Towards the future, the space mission CoRoT will also be partly dedicated to transit searches, and will be launched in late 2006. The advantages of space observations are: continuous and long time series and

more precise photometry. There will be 60,000 stars monitored during 150 days each, and 120,000 stars with shorter time series of about 25 days. The domain of “super-Earths” to Jupiters will be probed in planet radius, for planets at periods shorter than 50 days. CoRoT has the specificity of getting three-colour light curves, for 80% of the targets, which will help the discrimination of planetary transits against eclipsing binaries and stellar activity. The detection rate expected for CoRoT greatly depends on the frequency of “hot Neptunes” and on the actual target selection that will be done. Tentative estimates of CoRoT detections are described in references 8 and 41. The next space mission *Kepler*, with longer time series on a given field and a more sensitive instrument, will, a few years later, have the capability of discovering Earth sisters (similar period and size, around Sun-like stars) (9).

3.6 Biases of the method

The biases of the transit method are simply derived from the equations given in Sec. 2. The probability of observing the transit is larger for i) a large star, ii) a short star-planet distance. The second parameter is the most sensitive, since the star radius does not change by large factors along the main sequence. The star-planet distance also plays a role in the transit detection since it is directly related to the number of events present in a light curve for a given observing period. If the presence of three transits is a detection criterion (to establish the periodicity of the transit signal), it is obvious that shorter periods will be favored by having more than three transits within the observation window. The method is also biased towards larger planets, or smaller stars; both making the r/R ratio larger and thus producing a deeper transit signal. Finally, ground-based transit searches may also suffer an observing bias in detected planetary periods due to the Earth rotation. Periods being a multiple of Earth’s day are more favourable since several transits may be consecutively observed in good conditions (star elevation). This bias was recently evidenced by the hot Jupiters found in the OGLE survey (e.g. OGLE-TR- 111, ref. 45).

3.7 Eclipsing binaries and false positives

One conclusion of the ground-based photometric campaigns of OGLE was the high proportion of eclipsing binary stars which mimic a planetary transit: the transit depth, duration, and the orbital period resemble those expected for planets. A statistical analysis of such planetary transit mimics in transit surveys was proposed by Brown (16), comparing detection rates of planets and binaries of any types in ground-based and space-based transit searches. This kind of analyses show that, for any transit depths, the number of mimics is expected to be higher than the

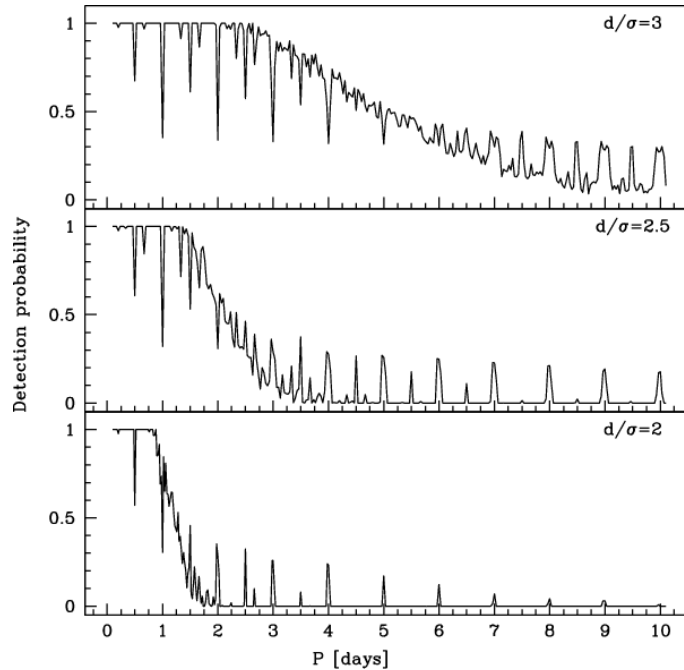


Figure 5.: *The detection probability against the orbital period, in the OGLE survey, according to Monte Carlo simulations, for three transit depths: 3, 2.5 and 2 times the dispersion of the photometric data.*

number of actual planetary transits. Several confusion scenarii may be distinguished:

Grazing binaries (Figure 7a). Two large stars, when eclipsing at an inclined angle, can produce shallow transit-like dips in the light curve. These cases produce, on average, rather deep signals in the light curve and are the easiest to discriminate. Several hints are usually present in the light curve itself, such as a V-shaped transit curve, ellipsoidal modulations due to tidal effects (24 and figure 8), or a mismatch between the transit duration and the transit depth assuming a planet-sized transiting body. Nevertheless, at low signal-to-noise such systems can also be mistaken for planetary transits. They are easy to resolve with spectroscopic observations, thanks to the presence of two sets of lines in the spectra with large velocity variations.

Small-radius stellar companion (Figure 7b). A small M-dwarf transiting a larger star can produce a photometric signal closely similar to a planetary transit. If the companion is not larger than a hot Jupiter,

and the orbital distance is too large for tidal and reflection effects to be detectable in the light curve, then the photometric signal is strictly identical to that of a planetary transit. Two examples of planet-sized stars were recently found, OGLE-TR-122 and OGLE-TR-123 (46, 47). Only radial-velocity follow-up of these transiting candidates has the capacity of resolving the nature of such systems.

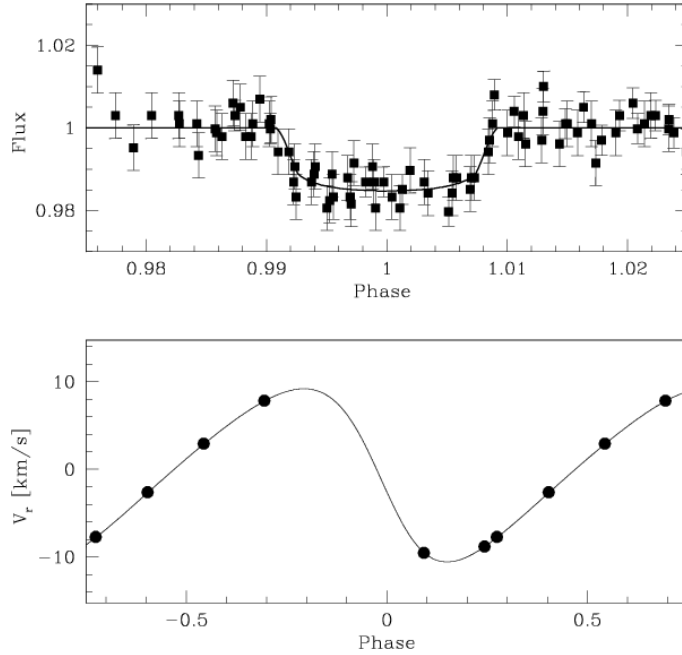


Figure 6.: *The phased light curve and radial-velocity curve of OGLE-TR-122, one of the transit candidates (62). The photometric curve precisely mimics the transit of a planet in front of a star, but the Doppler curve shows that the mass of the companion is not compatible with this scenario: it is a planet-size M dwarf (46).*

Note that such impostors among binary systems are generally those with a large temperature difference between components. The depths of the primary and secondary transits are different by a factor $(T_2/T_1)^4$, and in case of a binary with a hot primary star and a cool secondary, the primary transit will be much deeper than the secondary, as in a transiting planetary system. In the case of a binary with equal temperatures, however, both transits have the same depth, and then, the light curve could also mimic a transiting planet, with a period twice as short.

Eclipsing binaries which light is diluted by a third star (a foreground star, or a gravitationally bound triple system, Figure 7c). In most cases, multiple systems are readily discriminated with high-resolution spectroscopy from the presence of several systems of lines in the spectra. However, in some cases, the parameters can conspire not only to mimic the light curve of a planetary transit, but also to induce planet-like variations of the inferred radial velocity, produced by the blending of several sets of lines in the spectra. OGLE-TR-33 (59) is such a case. Another similar case was found in the TrES survey (38).

False positives (Figure 7d). They are patterns in the light curve, which are detected and wrongly identified as transit events. They may originate either from observational artefacts, instrumental features or stellar activity patterns. They can be recognized either by comparing other photometric data (e.g. in a second campaign on the same stellar field, with a low probability of finding the same artefact), or by RV follow-up (no RV signal associated to the transit phasing). Note that the blind test of transit detection performed for CoRoT light curves indicated a dependence of false positive detections on the method used (41). False positives were never identified on the same light curve by five independent teams. Also, efficient detrending such as performed by SYSREM (56) considerably decreases the false alarm rate.

3.8 Detection threshold

A recent study of the effect of the measurement noise in photometric surveys pointed out the importance of "red noise" (48). It shows that the usual assumption of white, independent noise to estimate the detection yields of transit surveys can be misleading. The contribution of covariant red noise is not negligible and must be accounted for as well. In the presence of red noise, the significance of a transit detection is:

$$SNR = \frac{\Delta F}{\sqrt{\frac{\sigma^2}{n} + \frac{\sum_{i \neq j} cov[i;j]}{n^2}}} \quad (8)$$

where σ is the photometric uncertainty on individual points, n is the number of data points during the transit, and $cov[i;j]$ are the elements of the covariance matrix. The origins of the covariant noise are atmospheric or instrumental fluctuations, which create systematics in light curves on the timescale of an hour. This limits considerably the detection rate of a given survey and yields predicted numbers which are in better adequation with the announced detection (49). The dependence on period and magnitude is also different than when only white noise is assumed. Figure 9 shows an example of transit detectability in the case

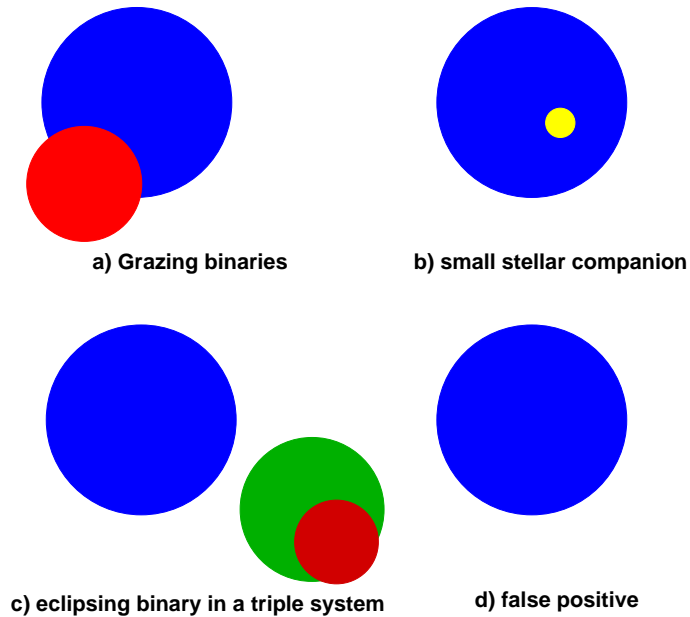


Figure 7.: *Sketches of confusion cases: a) grazing binaries, b) binaries with an M dwarf companion, c) binaries in a triple system, d) false positive (caused by stellar activity or instrumental feature).*

of the OGLE survey, when white noise is assumed, and when red noise is included. The difference between the two thresholds has a large effect on the expected rate of detection of hot Jupiter transits, since those are expected to produce typical transits near 1% depth, exactly in the region where the prediction of white noise and red noise diverge. Generally, taking the red component of the noise into account can result in a drastic downward revision of the expected yields.

4. Planet characterisation

The search for transits in a photometric survey requires a series of observing confirmations, most importantly RV observations. The combination of both techniques gives access to a rich determination of planetary parameters. Conversely, a photometric search for transits is always conducted on planets detected by radial velocity.

4.1 Planet confirmation

When planet candidates are proposed by transit surveys, it is necessary to perform additional observations to confirm the planetary origin

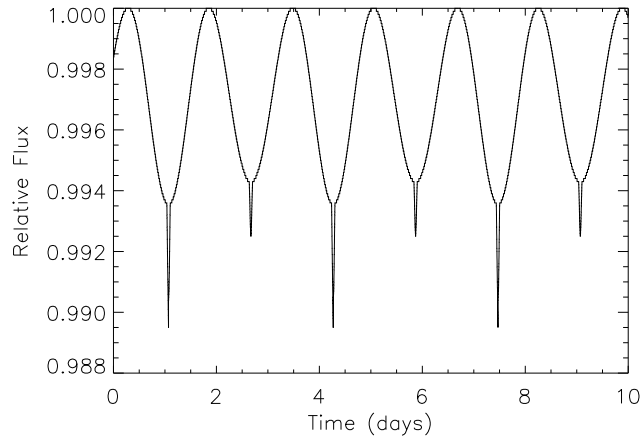


Figure 8.: *A grazing binary star light curve shows strong sinusoidal modulations in addition to the occultation, due to tidal effects. The case shown here corresponds to mass ratio 0.8 and period about 3 days. Such feature may help distinguish planetary and stellar transits.*

of the transit. As stated in previous sections, the number of impostors or false positives may be greater than the number of true planetary events. Radial-velocity follow-up of transit candidates has proven to be an efficient way of removing impostors (11, 44, 33), even if some of them may be identified on the light curve itself, searching for the secondary eclipse, V-shaped transits and sine-wave modulations, all effects typical of binary star light curves. A few RV data points are usually enough to identify grazing eclipsing binaries, since the amplitude of the RV variations is large. Blended systems or triple systems may be more tricky to identify. For the remaining candidates with low amplitudes in the RV curve, still compatible with planets, then the RV measurements provide an estimate of the true planetary mass. For edge-on systems, there is indeed no indetermination on the mass ($\sin i \simeq 1$).

4.2 Light curves of RV planets

Alternatively, one may discover a planet using the RV method and search for a potential transit. This is the way the first transiting planet HD 209458b was found (17), and more recently, the smaller planet HD 149026b (52) and the short-period HD 189733b (12). All short-period planets discovered in RV surveys are systematically monitored in photometry. Knowing the ephemeris and expected duration of the transit

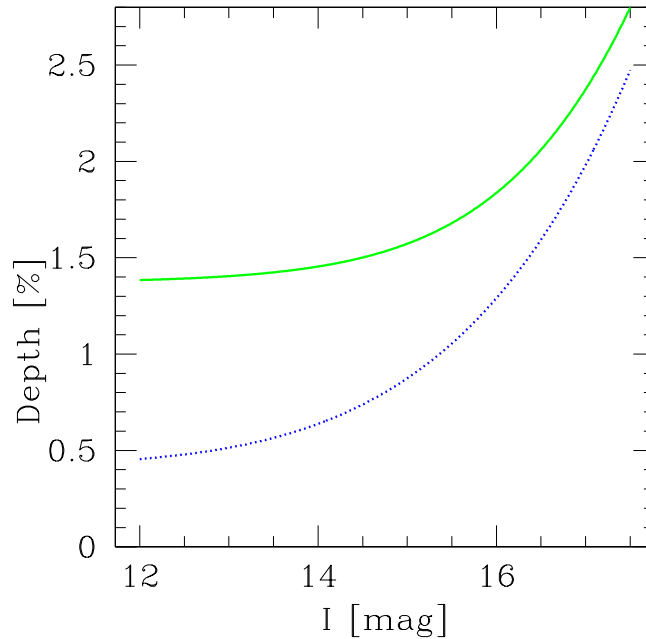


Figure 9.: *Detection threshold with (plain line) and without (dashed line) systematics, against magnitude, for a 3.5-day period planet in the OGLE survey (48).*

from the RV curve is a different problem than the blind search for transits in a wide set of light curves. Higher-sensitivity detections are possible, which is illustrated by the transit observations of HD 149026b, with a depth of only 3 mmag. Such shallow transits are probably missed, for sensitivity reasons, in wide transit surveys although the time series may contain several such events. The second advantage of observing transits around planets found by the RV technique is that the main target is bright enough to permit the observations of several “by-products”: the Rossiter-McLaughlin effect, the thermal emission during the secondary eclipse, the search for atmospheric elements in high-resolution spectra, etc... (see Section 4.4). Such detailed secondary observations of planets discovered by OGLE, or CoRoT in the future, are more difficult because the targets are fainter. New RV programs were recently initiated with the goal of detecting transiting short-period planets (20, 25); the strategy is to focus on metal-rich stars, for which the probability to detect a planet is 4 to 5 times larger than for stars with solar abundance (53).

4.3 The mass-radius diagram

One of the main product of transiting planet searches is to fill in the mass-radius diagram of transiting extrasolar planets (Table 1 and Figure 10). Theories of planet formation and evolution, and models of the internal structure of giant planets then benefit from essential constraints (28). For instance, the larger mass and smaller radius of shorter-period planets observed in Fig. 10 could be explained by the efficiency of the evaporation process (5). The M-R diagram of transiting extrasolar planets will get further populated by future transit searches (CoRoT, SuperWASP, *Kepler*, and continuations of OGLE and TrES, ...). From the large breakthrough done in the few past years, based on the first nine transiting planets, one can expect outstanding results may be expected in the field of exoplanetology from transiting planets in the near future.

Table 1.: *Parameters of all known and confirmed transiting extrasolar planets. References are in 33, 10, 45, 4, 52, 17, 30, 12, 34.*

Star name	Sp type	r	m	ρ	a	P
		R_{Jup}	M_{Jup}	g.cm^{-3}	AU	days
HD 209458	G0V	1.347	0.69	0.35	0.046	3.5248
HD 149026	G0IV	0.725	0.36	1.17	0.042	2.8766
HD 187933	K1V	1.26	1.1	0.69	0.03	2.219
OGLE-TR-56	G2V	1.23	1.45	1.0	0.0225	1.212
OGLE-TR-113	K2V	1.09	1.08	1.3	0.0228	1.43
OGLE-TR-132	F6V	1.13	1.19	1.02	0.0303	1.69
OGLE-TR-111	K1V	1.0	0.53	0.66	0.047	4.016
OGLE-TR-10	G0V	1.117	0.63	0.56	0.0416	3.10
TrES-1	K0V	1.08	0.75	0.74	0.0393	3.03

4.4 Further analysis of transiting planets

In addition to the transit caused by the planet body, one may study and characterise the transiting system through various secondary effects occurring in transiting planetary systems.

Thermal emission of the transiting planet. In transiting systems, a secondary eclipse (when the planet passes behind the star) also occurs except in extreme cases with very eccentric orbits. The secondary eclipse, however, is more difficult to detect in visible light, since the flux emitted by the planet (including reflection) is very small compared to the star's flux. But in the infrared, where the star/planet contrast is lower, the secondary eclipse may be detected. It offers a unique opportunity to estimate the effective temperature of the planet, by

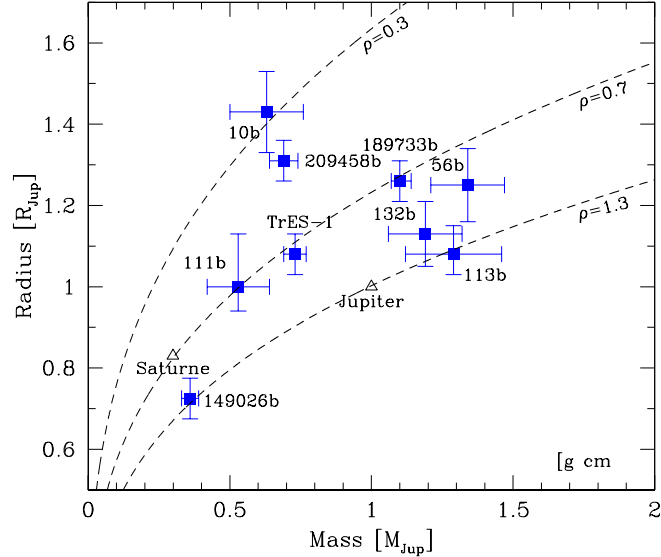


Figure 10.: *The mass-radius diagram of known transiting planets. Isodensity curves are also shown, and, for comparison, the location of Jupiter and Saturn.*

assuming that the depth of the secondary dip is the ratio of the planet emissivity over the star emissivity, modulated by the factor $(r/R)^2$. Recent detections of the thermal emission of the planets HD 209458b and TrES-1b give equilibrium temperatures of the order of 1000 K for these hot jupiter objects (19, 23).

Reflected light/Albedo. For planetary systems seen edge on, the light reflected by the planet surface is modulated by the phase angle α and depends on the geometric albedo p . The planet to star flux ratio f is then:

$$f(\alpha) = p \left(\frac{r}{a} \right) \left(\frac{\sin \alpha + (\pi - \alpha) \cos \alpha}{\pi} \right) \quad (9)$$

The first observing campaign on HD 209458 by the space photometric satellite MOST gave an upper limit of the geometrical albedo of the planet, which appears to be less than half as bright as Jupiter in the same bandpass (51). Such observations would give strong constraints

for the atmospheric models of giant planets. The latest transiting system HD 189733 has the most favorable set of parameters for a detection of this effect (its short period and late spectral type implies a reduced planet-star contrast).

Satellites and rings. The presence of a satellite orbiting the transiting planet may have a detectable imprint on the transit shape. Similarly, planetary rings have a signature on the transit light curve; ring features in transit light curves were recently investigated by Barnes and Fortney (6). These secondary effects, however, require a light curve with precision of about 10^{-4} , and a good temporal sampling. The detectability of such features is greater during ingress or egress (6).

Finally, the spectroscopy of the planetary system during a transit may also reveal some characteristics of the system:

The Rossiter-McLaughlin effect. During the transit, the planet sequentially blocks the light coming from different regions of the star disc. As the star rotates, this produces a distortion of the stellar lines (Figure 11). This effect, measured in RV curves, allows to derive the projected angle between the star-planet axis and the star spin axis, and the projected rotation velocity of the star. It was measured for the transiting planets HD 209458 (50) and HD 189733 (12), which both showed a common direction for the planetary orbit and the star rotation axis. It was also recently discussed analytically by Ohta et al. (42).

Detection of the extended planetary atmosphere. During the transit of the planetary body, signatures from the planet atmosphere may appear superimposed to the stellar spectrum. This implies that at high spectral resolution, the transit depth depends on the wavelength: as some atmospheric species (such as alkali metals) may absorb the starlight with strong absorbing efficiencies, the effective radius of the planet in these wavelengths will include a larger part of the atmosphere and be correspondingly higher. Several observing campaigns followed the discovery of HD 209458 in search for these transmissive atmospheric features. It turned out to be impossible from the ground, due to the contamination by the Earth's atmosphere, but gave striking results from space observatories. Atomic Sodium was first detected by HST observations (18), and then Hydrogen in the Ly α line, which showed a 15% depth (63), compatible with a high evaporation rate. More species were tentatively detected (oxygen and carbon, 64), which illustrates the potential of detailed observations of transiting systems to learn about the physics of exoplanetary atmospheres.

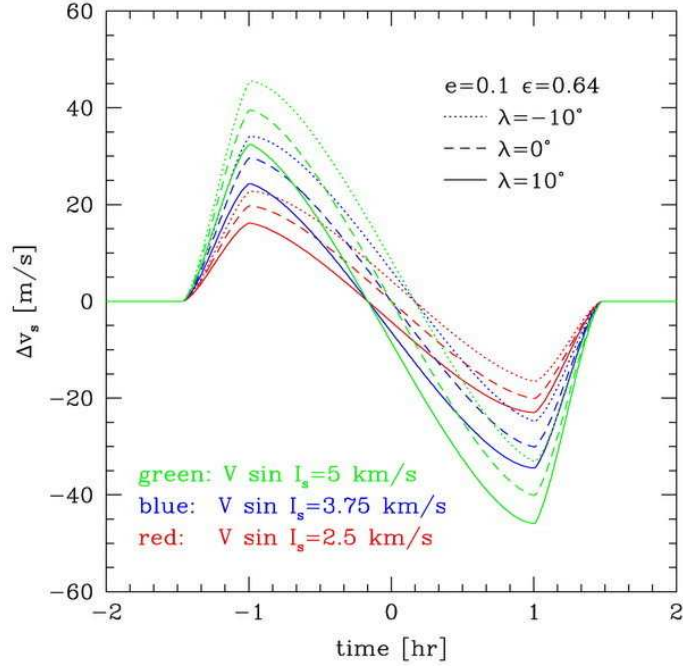


Figure 11.: The profile due to the Rossiter-McLaughlin effect shows up in the RV curve of a transiting planetary system at the transit epoch. This model curves for several system parameters are from Ohta et al. (42); λ is the projected angle between the planet orbital axis and the star spin axis.

5. Conclusion

The principles of the transit method for the detection and characterisation of extrasolar planets was presented. In summary, we may recall a few important facts:

- The radius of transiting planets is accurately determined (as long as the stellar radius is precisely known). Combined with radial-velocity measurements, it thus gives access to an estimate of the mean planetary density.
- Several scenarii of transit impostors complicate the detection and identification of candidates in large photometric surveys. A careful analysis of the light curve and follow-up observations are then required for confirmation.

- Transiting systems, especially when the star is bright and period is short, are ideal targets for performing additional observations and constrain: the effective temperature of the planet, its atmospheric composition and escape rate of its extended atmosphere, its albedo, or the presence of rings or satellites...

New transit candidates are currently searched for in dedicated ground-based photometric surveys and will soon be the targets of space missions: CoRoT launched in 2006, and *Kepler* to come next. Another extension of transit searches from the ground could be carried out in Antarctica, where the duty cycle is larger and skies potentially transparent and stable for high-accuracy photometry (26, 21). Expectations from all these searches are huge since they strongly constrain the physics, formation and evolution of irradiated planets, and in the longer term, they may yield the first detections of telluric planets. One must only keep in mind that transit detections should always be accompanied by a thorough strategy of complementary observations for the rejection of impostors and planet mass determination.

References

- [1] Aigrain, S. & Favata, F., 2002, A&A 395, 625
- [2] Alard, C. & Hupton, R.H., 1998, A&A 503, 325
- [3] Alard, C., 2000, A&AS 144, 363
- [4] Alonso, R., Brown, T., Torres, G. et al., 2004, ApJ 613, L153
- [5] Baraffe I., Selsis, F., Chabier, G. et al., 2004, A&A 419, L13
- [6] Barnes, J.W. & Fortney, J.J., 2004, ApJ 616, 1193
- [7] Bordé, P. 2003, PhD thesis,
<http://cfa-www.harvard.edu/~pborde/publications.html>
- [8] Bordé, P., Rouan, D. & Léger, A., 2003, A&A 405, 1137
- [9] Borucki, W. et al, 2004, in “Second Eddington Workshop”, ed. F. Favata, S. Aigrain and A. Wilson, p 177
- [10] Bouchy, F., Pont, F., Santos, N.C. et al, 2004, A&A 421, L13
- [11] Bouchy F., Pont, F., Melo, C. et al, 2005, A&A 431, 1105
- [12] Bouchy F., Udry, S., Mayor, M. et al, 2005, A&A 444, L15
- [13] Bramich, D.M., Horne, K., Bon, I.A. et al., 2005, MNRAS 359, 1096
- [14] von Braun, K., Lee, B.L, Seager, S. et al., 2005, PASP 117, 141
- [15] Brown, T., Charbonneau, D., Gilliland, R. et al, 2001, ApJ 552, 699

- [16] Brown, T., 2003, ApJ 593, L125
- [17] Charbonneau, D., Brown, T., Latham, D. et al, 2000, ApJ 529, L45
- [18] Charbonneau, D., Brown, T., Noyes, R. et al, 2002, ApJ 568, 377
- [19] Charbonneau, D., Allen, L., Megeath, T. et al., 2005, ApJ 626, 523
- [20] Da Silva R. et al., 2005, A&A in press
- [21] Deeg, H., Alonso, R., Belmonte, J.A. et al., 2004, PASP 116, 985
- [22] Defaÿ, C., Deleuil, M. & Barge, P., 2001, A&A 365, 330
- [23] Deming, D. et al., 2005, Nature 434, 740
- [24] Drake, A.J., 2003, ApJ 589, 1020
- [25] Fischer D., Laughlin, G., Butler, P. et al, 2005, ApJ 620, 481
- [26] Fressin, F., Guillot, T., Bouchy, F. et al., 2005, EAS pub. series 14, 309
- [27] Gilliland, R.L., Brown, T.M., Guhathakurta, P. et al., 2000, ApJ 545, L47
- [28] Guillot, T., 2005, Ann. Rev. of Earth and Plan. Sc., 33, 493
- [29] Hartman, J. D., Stanek, K. Z., Gaudi, B. S. et al., 2005, AJ 130, 2241
- [30] Henry, G.W., Marcy, G., Butler, P. et al, 2000, ApJ 529, L41
- [31] Horne, K., 2003, in “Scientific Frontiers in Research on Extrasolar Planets”, ASPC 294, ed. D. Deming and S. Seager, p361
- [32] Jenkins, J.M., 2002, ApJ 564, 495
- [33] Konacki, M. et al., 2003, ApJ 597, 1076
- [34] Konacki, M., Torres, G., Sasselov, D. et al, 2005, ApJ 624, 372
- [35] Kovács, G., Zucker, S. & Mazeh, T., 2002, A&A 391, 369
- [36] Mandel, K. & Agol, E., 2002, ApJ 580, L171
- [37] Mallén-Ornelas, G., Seager, S., Yee, H. et al., 2003, ApJ 582, 1123
- [38] Mandushev G., Torres G., Latham D.W. et al. 2005, ApJ 621, 1061
- [39] Mochejska, B. J., Stanek, K. Z., Sasselov, D.D. et al., 2005, AJ 129, 2856
- [40] Moutou, C. , Pont, F., Bouchy, F. et al., 2004, A&A 424, L31
- [41] Moutou, C., Pont, F., Barge, P. et al., 2005, A&A 437, 355
- [42] Ohta, Y., Taruya, A. & Suto, Y., 2005, ApJ 622, 1118
- [43] Pepper, J. & Gaudi, B.S., 2005, ApJ 631, 581

- [44] Pont, F., Bouchy, F., Melo, C. et al, 2005, A&A 438, 1123
- [45] Pont, F., Bouchy, F., Queloz, D. et al, 2004, A&A 426, L15
- [46] Pont, F., Melo, C., Bouchy, F. et al, 2005, A&A 433, L21
- [47] Pont, F., Moutou, C., Bouchy, F. et al, 2005, in press
- [48] Pont, F., 2005, in "Tenth Anniversary of 51Peg-b", eds. Arnold, Bouchy and Moutou, Platypus Press.
- [49] Pont, F. & Zucker, S., 2006, in prep.
- [50] Queloz, D., Eggenberger, A., Mayor, M. et al., 2000, A&A 359, L13
- [51] Rowe, J. et al., 2005, in press
- [52] Sato, B., Fischer, D., Henry, G. et al., 2005, ApJ 633, 465
- [53] Santos, N.C., Israelian, G., mayor, M. et al., 2005, A&A 437, 1127
- [54] Seager, S. and Mallen-Ornelas, G., 2003, ApJ 585, 1038
- [55] Street, R.A., Horne, K., Lister, T.A. et al., 2003, MNRAS 340, 1287
- [56] Tamuz, O., Mazeh, T., Zucker, S., 2005, MNRAS 356, 1466
- [57] Tingley, B., 2003, A&A 408, L5
- [58] Tingley, B. & Sackett, P., 2005, ApJ 627, 1011
- [59] Torres G., Konacki M., Sasselov D. 2004, ApJ, 614, 979
- [60] Udalski A., et al., 2002, Acta Astron. 52, 217
- [61] Udalski A., et al., 2002b, Acta Astron. 52, 317
- [62] Udalski A., et al., 2003, Acta Astron. 53, 133
- [63] Vidal-Madjar, A., Lecavelier des Etangs, A., Désert, J.-M. et al., 2003, Nature 422, 143
- [64] Vidal-Madjar, A., Désert, J.-M., Lecavelier des Etangs, A. et al., 2004, ApJ 604, L69